ACSNANO
www.acsnano.org
ARTICLE

Layer Control of WSe_2 *via* Selective Surface Layer Oxidation

Zhen Li,[†] Sisi Yang,[‡] Rohan Dhall,[†] Ewa Kosmowska,[§] Haotian Shi,[∥] Ioannis Chatzakis,[†] and Stephen B. Cronin*[,†,‡,∥]

Departments of [†]Electrical Engineering, [‡]Physics and Astronomy, and [∥]Chemistry, University of Southern California, Los Angeles, California 90089, United States

[§]XEI Scientific, Redwood City, California 94063, United States

Supporting Information

ABSTRACT: We report Raman and photoluminescence spectra of mono- and few-layer WSe_2 and $MoSe_2$ taken before and after exposure to a remote oxygen plasma. For bilayer and trilayer WSe_2, we observe an increase in the photoluminescence intensity and a blue shift of the photoluminescence peak positions after oxygen plasma treatment. The photoluminescence spectra of trilayer WSe_2 exhibit features of a bilayer after oxygen plasma treatment. Bilayer WSe_2 exhibits features of a monolayer, and the photoluminescence of monolayer WSe_2 is completely absent after the oxygen plasma treatment. These changes are observed consistently in more than 20 flakes. The mechanism of the changes observed in the photoluminescence spectra of WSe_2 is due to the selective oxidation of the topmost layer. As a result, *N*-layer WSe_2 is reduced to $N-1$ layers. Raman spectra and AFM images taken from the WSe_2 flakes before and after the oxygen treatment corroborate these findings. Because of the low kinetic energy of the oxygen radicals in the remote oxygen plasma, the oxidation is self-limiting. By varying the process duration from 1 to 10 min, we confirmed that the oxidation will only affect the topmost layer of the WSe_2 flakes. X-ray photoelectron spectroscopy shows that the surface layer WO_x of the sample can be removed by a quick dip in KOH solution. Therefore, this technique provides a promising way of controlling the thickness of WSe_2 layer by layer.

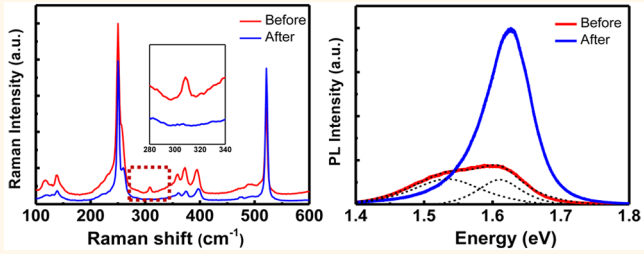

KEYWORDS: *dichalcogenide, WSe_2, $MoSe_2$, photoluminescence, oxygen plasma, oxidation*

Two-dimensional transition metal dichalcogenides (TMDCs), such as MoS_2, WSe_2, and $MoSe_2$, have demonstrated great optical properties and the potential for future applications in electronic and optoelectronic devices. Various devices based on TMDCs have been demonstrated, including field-effect transistors (FETs),[1] photodetectors,[2,3] and light-emitting diodes (LEDs).[4−6] One of the unique optical properties of these TMDCs is the indirect-to-direct band gap transition that occurs when the thickness of these materials is changed from bulk to a monolayer flake. Monolayer TMDCs are direct band gap semiconductors exhibiting strong photoluminescence (PL), and few-layer TMDCs are indirect semiconductors, in which the luminescent properties are strongly suppressed.[7−9] Because of the two-dimensional nature and high surface-to-volume ratio of TMDCs, surface states and interaction with the substrate are particularly important in these two-dimensional material systems. Previously, various passivation methods have been used to improve both the carrier mobility and luminescence efficiency of TMDCs, including atomic layer deposition (ALD),[1] hexagonal boron nitride encapsulation,[10−13] and immersion in ionic liquid solutions.[14,15] Yamamoto *et al.* studied the selective oxidation of WSe_2 after exposure to O_3 at 100 °C for a few hours.[16] While the formation of a uniform surface oxide is advantageous by providing protection from environmental effects and providing a good seed layer for ALD of high-*k* dielectrics, this previous ozone treatment also resulted in a decrease in the PL intensity, indicating damage to the underlying layers of the material.

Low-power, remote oxygen plasmas are known to remove hydrocarbons from delicate sample surfaces that are susceptible to damage by the highly energetic ions in the plasma.[17,18] In our previous work,[19] we reported oxygen-plasma-induced layer decoupling of few-layer MoS_2 and an associated enhancement in the PL intensity. In the work presented here, we investigate the effect of this gentle oxygen plasma treatment on transition metal selenides, WSe_2 and $MoSe_2$. Unlike the sulfide, a homogeneous single-layer oxidation is grown on the surface of the WSe_2 flakes after the treatment. Compared to O_3

Received: April 12, 2016
Accepted: July 8, 2016
Published: July 8, 2016

DOI: 10.1021/acsnano.6b02488
ACS Nano 2016, 10, 6836−6842

exposure,[16] the remote oxygen plasma treatment presents an easier and more controllable approach, which causes less damage to the WSe_2 flakes. In total, we compare 27 WSe_2 flakes and 15 $MoSe_2$ flakes before and after the treatment, with different plasma exposure times ranging from 1 to 10 min. The PL and Raman spectra show very consistently that only the first layer on the surface of the WSe_2 flake is oxidized during the plasma treatment. The oxygen ions do not penetrate further into the flake and oxidize the underlying layers, even with longer exposure times. The PL intensity of WSe_2 and $MoSe_2$ after the treatment is increased by up to 6-fold, further indicating that the underlying layers of WSe_2 are not affected significantly by oxygen plasma. To confirm the oxidation of the WSe_2 samples, we performed X-ray photoelectron spectroscopy (XPS) of WSe_2 before and after the oxygen plasma treatment.

In this experiment, we start by exfoliating WSe_2 and $MoSe_2$ flakes onto Si substrates with 300 nm oxide. Based on the contrast observed in an optical microscope, we select different WSe_2 samples ranging from one monolayer to a few layers in thickness. Raman and photoluminescence spectroscopy are used to confirm the layer number of a given flake.[20−22] After finishing the characterization of the pristine samples, we performed oxygen plasma treatment with an Evactron plasma decontaminator designed by XEI Scientific, Inc. In typical plasma cleaners (*i.e.*, ashers), the sample is bombarded with ions carrying significant kinetic energy, resulting in a "sputtering" mechanism that is detrimental to these delicate 2D-layered materials. Remote plasma cleaners, on the other hand, rely mainly on the chemical reactivity of the oxygen radicals. Here, the sample is placed 10 cm away from the plasma. By the time the oxygen radicals diffuse to the sample, they have lost most of their kinetic energy but retain their chemical reactivity.

Figure 1a shows optical microscope images of bilayer and trilayer WSe_2 flakes deposited on the Si/SiO_2 substrate taken before and after the oxygen plasma treatment. As previous studies have shown,[21,23] the bulk $^1B_{2g}$ Raman mode at 310 cm^{-1} does not exist in monolayer WSe_2 and is only observed in multilayer and bulk WSe_2. The Raman spectra of bilayer WSe_2 taken before and after oxygen plasma treatment (plotted in Figure 1b) show that this Raman mode disappears after the treatment. In addition, monolayer WSe_2 only exhibits a single PL peak around 1.63 eV, while bilayer WSe_2 has two PL peaks at lower energies, 1.53 and 1.61 eV.[20] Here, both the Raman (Figure 1b) and PL spectra (Figure 1c) before and after oxygen plasma indicate that the bilayer WSe_2 flake is converted into monolayer WSe_2, and the flake is changed from an indirect to a direct band gap semiconductor. As a result, there is a 5-fold increase in the PL intensity. Besides surface oxidation, there are a few other mechanisms that can cause a bilayer-to-monolayer transition and the disappearance of the bulk $^1B_{2g}$ Raman mode. For example, interlayer decoupling can be induced by oxygen intercalation, as we observed in few-layer MoS_2.[19] In order to confirm that oxidation occurs in WSe_2, we further investigate PL, Raman, and XPS spectra of monolayer, trilayer, and few-layer WSe_2 flakes before and after oxygen plasma treatment.

Figure 2a,b shows the Raman spectra of monolayer and trilayer WSe_2 flakes before and after the oxygen treatment. For monolayer WSe_2, there is no $^1B_{2g}$ Raman mode at 310 cm^{-1}. If the oxygen plasma introduces oxygen intercalation between the WSe_2 layers, the trilayer WSe_2 would also behave like a monolayer after the plasma treatment. However, the 310 cm^{-1} peak remains in the Raman spectra of trilayer WSe_2 after the

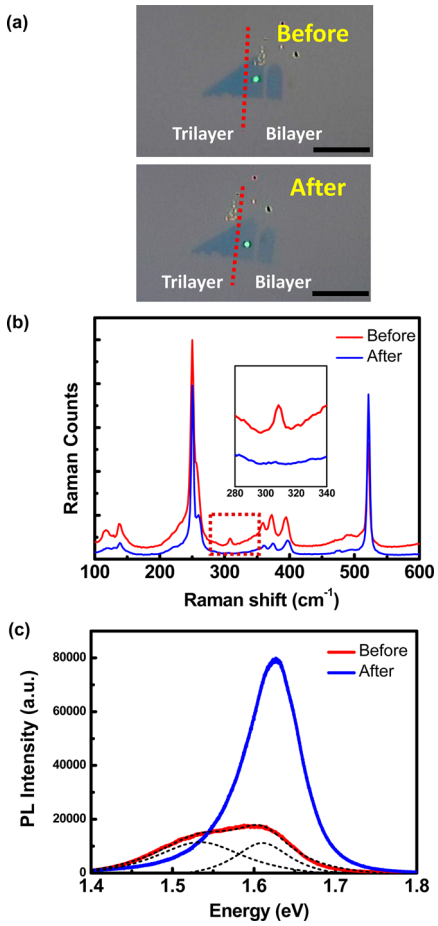

Figure 1. (a) Optical images of bilayer and trilayer WSe_2 flakes before and after the oxygen plasma treatment. The scale bar is 5 μm. (b) Raman spectra of the bilayer WSe_2 flake taken before and after the oxygen plasma treatment. The inset shows the bulk $^1B_{2g}$ Raman mode of WSe_2 at 310 cm^{-1}, indicating that the bilayer WSe_2 flake is converted into a monolayer after the oxygen plasma treatment. (c) Photoluminescence spectra of WSe_2 before and after the oxygen plasma treatment, also indicating a bilayer-to-monolayer transition.

treatment. In the trilayer WSe_2, there are also two main PL peaks. The higher-energy peak remains at a position similar to that of bilayer WSe_2 (1.61 eV), while the lower-energy peak is observed at 1.47 eV before oxygen plasma treatment.[20] After the treatment, the PL peaks shift to 1.51 and 1.61 eV, corresponding to bilayer emission, as shown in Figure 2d. For monolayer WSe_2, on the other hand, no Raman or PL signal can be observed (Figure 2c) after the oxygen plasma treatment. The absence of Raman peaks indicates that the monolayer has been mostly oxidized.

As mentioned above, in typical plasma cleaners used in semiconductor processing, the sample is bombarded with ions that may cause physical damage and thinning effects. To verify that the WSe_2 monolayer is not "etched" away but is instead oxidized after the remote oxygen plasma, atomic force microscope (AFM) images are taken from WSe_2 flakes before and after treatment, as shown in Figure 3. From the AFM images of monolayer and bilayer pristine and oxidized WSe_2 flakes, we found that the thickness of WSe_2 flakes remains the same after the treatment. Although both Raman and PL spectra identified the WSe_2 sample in Figure 3a as monolayer before treatment, the thickness measured from the AFM image is

DOI: 10.1021/acsnano.6b02488
ACS Nano 2016, 10, 6836−6842

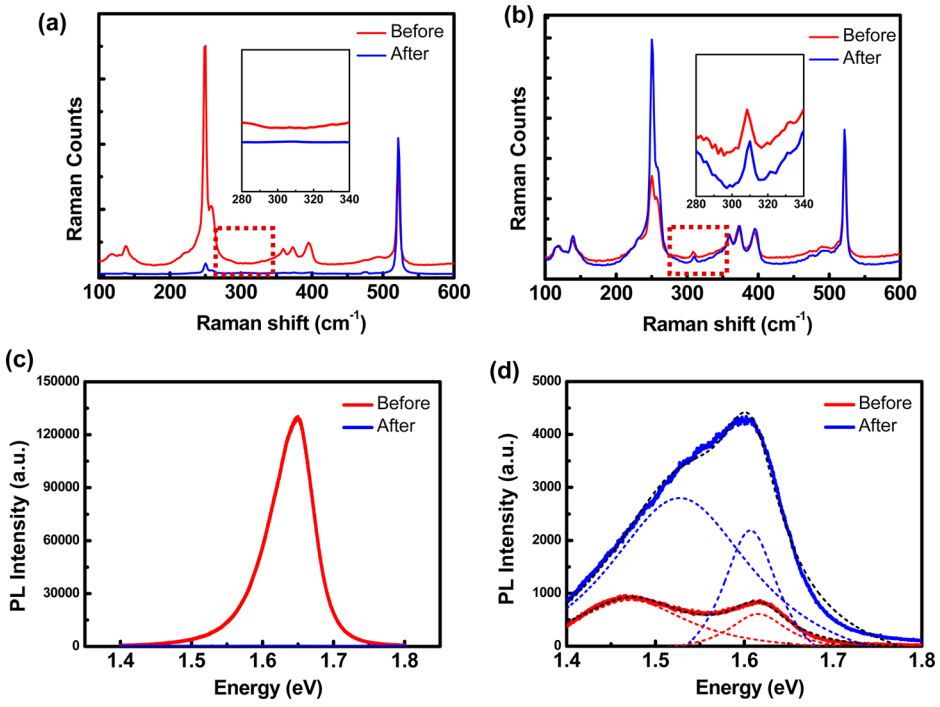

Figure 2. Raman spectra of the (a) monolayer and (b) trilayer WSe_2 flakes taken before and after the oxygen plasma treatment. Inset: Raman mode of WSe_2 at 310 cm^{-1}, which is not exhibited in monolayer WSe_2. Photoluminescence spectra of (c) monolayer and (d) trilayer WSe_2 before and after the oxygen plasma treatment. The two PL peaks of trilayer WSe_2 at 1.47 and 1.61 eV shift to 1.53 and 1.61 eV, corresponding to bilayer WSe_2. Monolayer WSe_2 is oxidized completely, and no PL signal is observed after the plasma treatment.

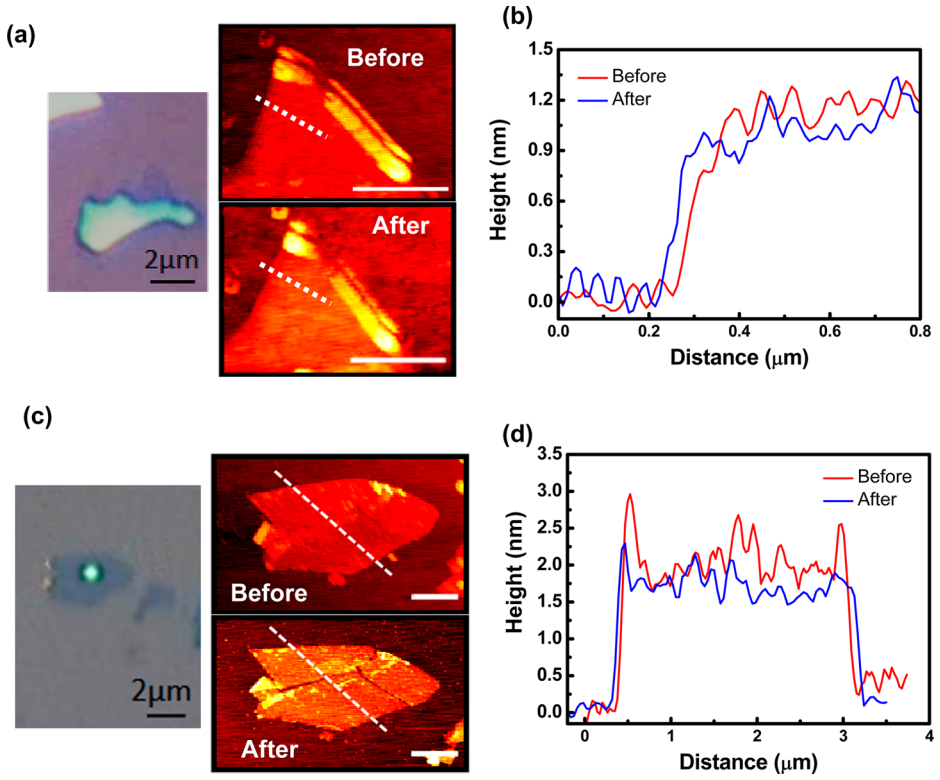

Figure 3. Optical and AFM images of (a) monolayer and (c) bilayer before and after the oxygen plasma treatment. The scale bar in the AFM images is 1 μm. Height profiles of WSe_2 (b) monolayer and (d) bilayer flakes before and after the treatment, along the white dashed lines in (a) and (c), respectively, show that the process does not change the thickness of the flake by a significant amount.

thicker than theoretical thickness of a monolayer WSe_2, 0.7 nm. This may be caused by the differences in gradients of the attractive forces and lateral forces on the material and the substrate, which has been reported on both graphene and MoS_2 before.[24−27] The fact that there is no observable decrease in the thickness of monolayer and bilayer WSe_2 samples before and

DOI: 10.1021/acsnano.6b02488
ACS Nano 2016, 10, 6836−6842

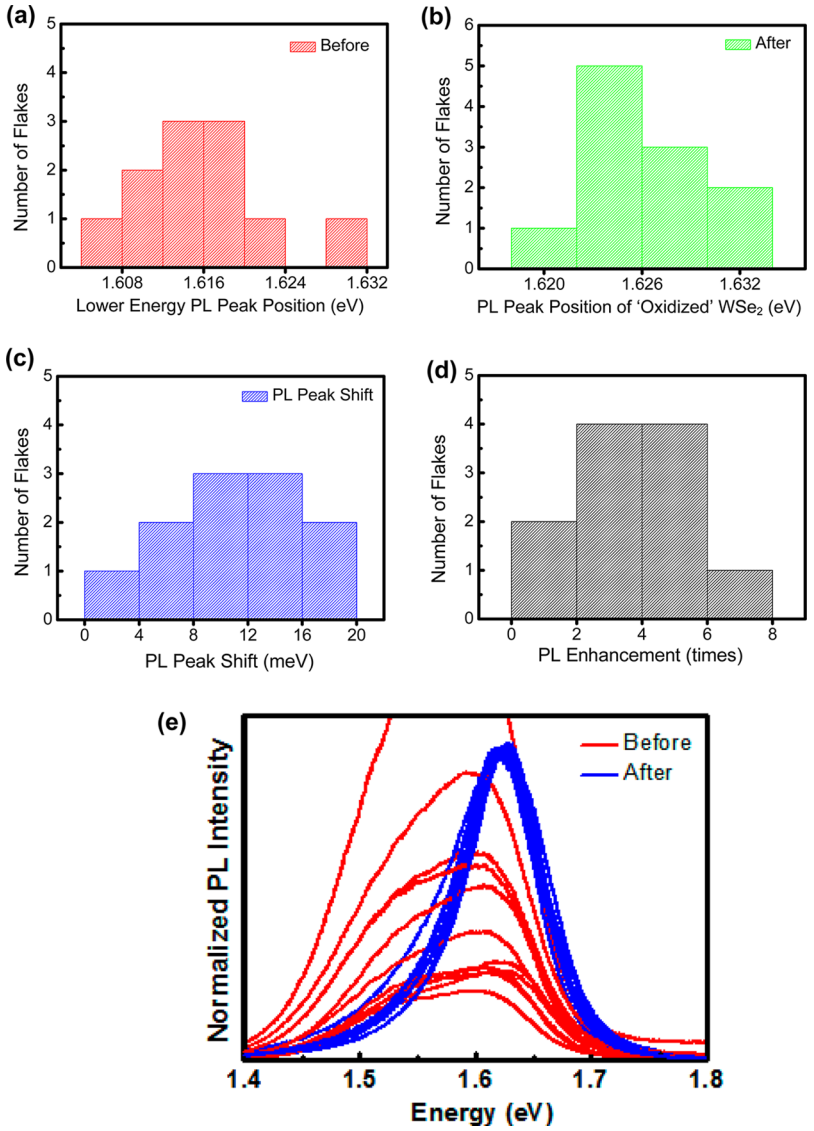

Figure 4. Histograms of bilayer WSe_2 PL peak position (the lower-energy peak) (a) before and (b) after the oxygen plasma treatment. (c) Shift in PL peak position before and after treatment. (d) PL intensity increase due the indirect-to-direct band gap transition. (e) PL spectra normalized by the PL peak intensity at 1.63 eV of 11 bilayer WSe_2 flakes taken before and after the oxygen plasma treatment.

after treatment suggests that the topmost WSe_2 layer is not removed due to physical bombardment. In addition, the AFM images show that the oxide film is uniform and does not change the surface topology (*i.e.*, roughness) of the material as compared to other dielectric layers deposited, for example, by ALD.[28]

RESULTS AND DISCUSSION

Among the 27 WSe_2 flakes that were compared before and after the oxygen plasma treatment, 11 out of 11 WSe_2 bilayer flakes became monolayer according to Raman and PL results. For all 11 of these flakes, the 310 cm^{-1} Raman peak disappeared, and the PL spectra changed from two peaks to one peak centered around 1.63 eV. Seven out of seven trilayer WSe_2 flakes were converted to bilayers, and five out of six monolayer WSe_2 flakes were completely oxidized, exhibiting no PL signal after plasma treatment. The oxygen plasma treatment had very little effect on the three remaining thicker WSe_2 flakes (more than five layers) because the properties of N-layer and $N-1$-layer WSe_2 are very similar when N is a large number. Figure 4a–d shows histograms of the PL intensity and peak position of bilayer WSe_2 before and after oxygen plasma treatment. The PL spectra of bilayer WSe_2 flakes can be fitted with two peaks, one at 1.53 eV and the other at 1.61 eV. We used the lower-energy PL peak to compare with the "monolayer" PL peak after treatment. Due to the indirect-to-direct band gap transition, the PL peak is blue-shifted and the PL intensity is increased. A similar analysis for trilayer WSe_2 samples can be found in Figure S4 in the Supporting Information. An average blue shift of 40 meV of the lower-energy PL peak is observed in the trilayer WSe_2 samples after the oxygen plasma treatment, consistent with bilayer emission. These statistics show very reliably that bilayer WSe_2 flakes are reduced to monolayers, and trilayer WSe_2 flakes become bilayers. Figure 4e shows the normalized PL spectra of bilayer WSe_2 samples before and after the oxygen plasma treatment. For all samples, the PL peak after the oxygen plasma treatment is blue-shifted to 1.63 eV consistently, and the PL intensity is increased for all samples except one. To examine the time dependence of the oxygen plasma treatment, we varied the duration of the plasma from 1

DOI: 10.1021/acsnano.6b02488
ACS Nano 2016, 10, 6836–6842

to 10 min. The Raman, PL, and XPS results show no significant difference in these two cases (see Figure S5), indicating that the oxidation is surface-saturated on the topmost layer, and the diffusion rate of excited oxygen radicals into the underlying WSe_2 layers is much smaller compared to the reaction rate between the oxygen and the surface layer. As a result, the process is self-limited. More detailed information, including PL and Raman spectra measured from monolayer, bilayer, and trilayer flakes, can be found in the Supporting Information.

Since only the top WSe_2 layer is affected by the oxygen plasma treatment, the oxide is amorphous rather than crystalline. As a result, no WO_2 or WO_3 Raman peaks are observed from the oxidation layer. Instead, we performed XPS of WSe_2 before and after oxygen plasma exposure. Figure 5 shows XPS spectra of the W_{4f} core level of an exfoliated WSe_2 sample before and after oxygen plasma treatment. The XPS spectrum of as-exfoliated WSe_2 shows the $4f_{7/2}$ and $4f_{5/2}$ features at 31.7 and 33.7 eV, corresponding to selenide-bonded tungsten.[29] After the oxygen treatment, the XPS spectrum measured from the same sample shows the emergence of weaker doublet peaks at 35.0 and 37.1 eV, in addition to the stronger selenide-bonded tungsten peaks at 31.7 and 33.7 eV. The larger binding energy doublet corresponds to $4f_{7/2}$ and $4f_{5/2}$ tungsten oxide (WO_x with $x \leq 3$).[30−32] To confirm that there is only surface oxidation, the WSe_2 sample was quickly dipped into a 1 mol/L KOH solution for less than 3 s to remove the surface oxide. After the dip in this base, the WO_x doublet peaks disappear, suggesting that the surface oxide layer is removed by the KOH solution.

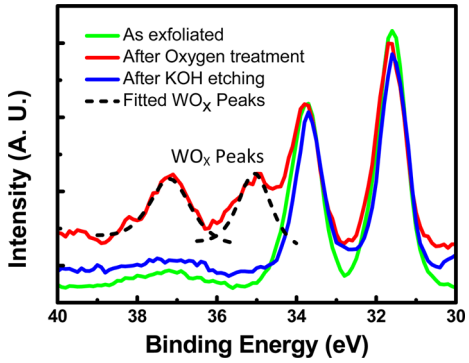

Figure 5. XPS spectra of tungsten 4f core level of the WSe_2 exfoliated sample before and after the oxygen plasma treatment and after a quick dip in 1 mol/L KOH solution to remove the surface oxide. The 31.7 and 33.7 eV peaks correspond to the WSe_2. After the oxygen plasma treatment, two additional peaks with larger binding energies appear at 35.0 and 37.1 eV, corresponding to $4f_{7/2}$ and $4f_{5/2}$ tungsten oxide (WO_x with $x \leq 3$). After a quick dip in 1 mol/L KOH solution, the same sample is measured again, and no oxide peaks are observed.

Similar effects of the remote oxygen plasma treatment are also observed in $MoSe_2$ flakes. Figure 6 shows Raman and PL spectra of a $MoSe_2$ flake before and after the oxygen plasma treatment. The intensity of the Raman peak near 360 cm^{-1} is reduced after the treatment, which can be assigned to the B_{2g} mode.[20] As with WSe_2, the B_{2g} mode is only observed in few-layer $MoSe_2$ flakes but is absent in monolayer $MoSe_2$. As shown in Figure 6, the disappearance of the B_{2g} Raman peak of the $MoSe_2$ after the treatment suggests a bilayer-to-monolayer transition. A blue shift in the PL peak from 1.52 to 1.57 eV is observed after the oxygen plasma treatment. Also, the PL intensity is increased by more than 3-fold. This plasma treatment will not affect few-layer $MoSe_2$ flakes thicker than five layers. Additional PL spectra of $MoSe_2$ flakes taken before and after the oxygen plasma treatment are included in Figure S6 in the Supporting Information. A consistent blue shift of the PL peak position and increase of the PL intensity is observed from $MoSe_2$ samples after the oxygen plasma treatment. These results imply that the selective surface oxidation by remote oxygen plasma may be applied to other transition metal selenide materials and, in general, may serve as a self-limiting oxidation technique for other TMDCs.

CONCLUSION

In summary, we demonstrate that a remote oxygen plasma treatment provides a self-limiting oxidation of the surface layer of WSe_2 and $MoSe_2$. Consequently, monolayer WSe_2 samples are oxidized completely, bilayer WSe_2 flakes become monolayer, and, in general, N-layer WSe_2 is reduced to $N-1$ layers, as established by Raman and PL spectra measured before and after the plasma treatment process. The PL intensity measured from "oxidized" bilayer WSe_2 is increased by as much as 6× and is comparable to pristine monolayer WSe_2, which indicates that the remote oxygen radicals do not penetrate beyond the topmost layer. It is somewhat surprising that the oxygen radical chemistry is different for transition metal selenides (WSe_2, $MoSe_2$) and sulfides (MoS_2), even though they come from the same column of the periodic chart. Compared to other layer-

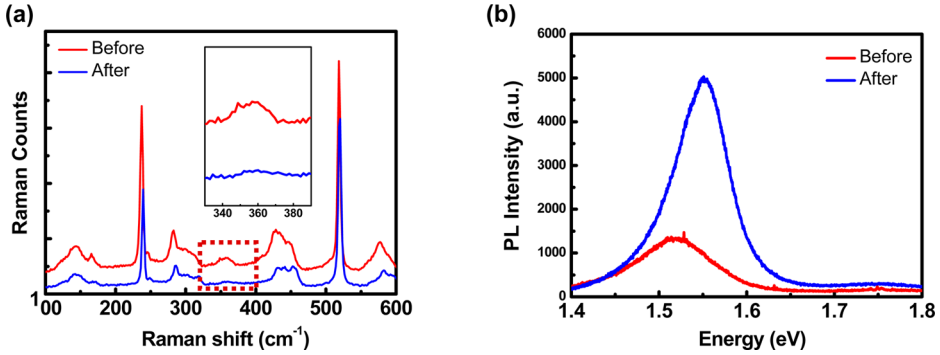

Figure 6. (a) Raman spectra of the bilayer $MoSe_2$ flake taken before and after the oxygen plasma treatment. The inset shows the B_{2g} Raman mode of $MoSe_2$ around 360 cm^{-1}. (b) Photoluminescence spectra of $MoSe_2$ before and after the oxygen plasma treatment. The PL peak blue shifts from 1.52 to 1.57 eV.

DOI: 10.1021/acsnano.6b02488
ACS Nano 2016, 10, 6836−6842

by-layer thinning methods of graphene and TMDCs,[33−35] the remote oxygen plasma treatment relies on chemical oxidation rather than physical bombardment. The kinetic energy of the oxygen radicals is very low, which makes it hard for them to penetrate the top layer oxide, resulting in a self-limiting process. This treatment will only oxidize one layer of WSe_2, even when we increase the treatment duration to 10 min, and the oxide can later be removed by KOH solution. The surface oxide layer may be advantageous for electronic devices, providing protection from environmental effects and as an effective hole injection layer to WSe_2.[36] In addition, this surface will likely serve as a good seed layer for atomic layer deposition of high-*k* dielectrics to improve the ALD/TMDC interface and the quality of the dielectric film.[28,37]

METHODS

Preparation of Single- and Few-Layer TMDC Films. Monolayer and few-layer WSe_2 and $MoSe_2$ films were exfoliated from bulk WSe_2 (HQ Graphene) and $MoSe_2$ (2Dsemiconductors Inc.) onto oxidized Si substrates containing lithographically defined grid markers by the widely used "Scotch tape" method.[26]

Raman and Photoluminescence Spectroscopy. Raman and photoluminescence spectra were taken using a Renishaw InVia spectrometer with a 532 nm laser (10 μW) focused through a 100× objective lens. Raman and PL spectra were collected at room temperature under ambient conditions. Optical images of the laser spot positions were recorded to ensure that the spectra were measured at the same location of the flake before and after the oxygen plasma treatment.

Oxygen Plasma Treatment. WSe_2 and $MoSe_2$ samples were exposed to a remote oxygen plasma for 2−5 min at a pressure of 200 mTorr using ambient air. The plasma power was set to 15 W. Despite the presence of nitrogen in the gas mixture, the plasma itself mainly consisted of oxygen radicals since the N_2 molecules have a much higher bond strength. The samples were placed at a distance of 10 cm from the plasma source to avoid direct bombardment from the highly energetic oxygen ions.

X-ray Photoelectron Spectroscopy. As-exfoliated, after oxygen treatment, and after a KOH dip, WSe_2 samples were investigated using a Kratos Axis Ultra DLD (X-ray photoelectron spectrometer). The instrument has a typical sampling depth of 2−3 nm. The *z*-height of the samples was focused using a green laser spot (rough alignment), and the O 1s signal was counted (fine alignment) to make sure the samples were focused by the X-ray. The binding energy range we explored for tungsten was from 40 to 23 eV, and ten 60 s sweeps were collected.

ASSOCIATED CONTENT

Supporting Information

The Supporting Information is available free of charge on the ACS Publications website at DOI: 10.1021/acsnano.6b02488.

PL spectra of monolayer and trilayer WSe_2, Raman spectra of bilayer WSe_2, statistical analysis of PL peak shifts of bilayer and trilayer WSe_2 flakes, and PL spectra of $MoSe_2$ flakes (PDF)

AUTHOR INFORMATION

Corresponding Author

*E-mail: scronin@usc.edu.

Notes

The authors declare no competing financial interest.

ACKNOWLEDGMENTS

This research was supported by Department of Energy (DOE) Award No. DE-FG02-07ER46376 (Z.L.) and NSF Award No. 1402906. (S.Y.). The authors thank Dr. Marcos Pimenta for useful insight and discussions.

REFERENCES

(1) Radisavljevic, B.; Radenovic, A.; Brivio, J.; Giacometti, V.; Kis, A. Single-Layer MoS_2 Transistors. *Nat. Nanotechnol.* **2011**, *6*, 147−150.
(2) Yin, Z.; Li, H.; Li, H.; Jiang, L.; Shi, Y.; Sun, Y.; Lu, G.; Zhang, Q.; Chen, X.; Zhang, H. Single-Layer MoS_2 Phototransistors. *ACS Nano* **2012**, *6*, 74−80.
(3) Lopez-Sanchez, O.; Lembke, D.; Kayci, M.; Radenovic, A.; Kis, A. Ultrasensitive Photodetectors based on Monolayer MoS_2. *Nat. Nanotechnol.* **2013**, *8*, 497−501.
(4) Baugher, B. W.; Churchill, H. O.; Yang, Y.; Jarillo-Herrero, P. Optoelectronic Devices based on Electrically Tunable *pn* Diodes in a Monolayer Dichalcogenide. *Nat. Nanotechnol.* **2014**, *9*, 262−267.
(5) Pospischil, A.; Furchi, M. M.; Mueller, T. Solar-energy Conversion and Light Emission in an Atomic Monolayer *pn* Diode. *Nat. Nanotechnol.* **2014**, *9*, 257−261.
(6) Ross, J. S.; Klement, P.; Jones, A. M.; Ghimire, N. J.; Yan, J.; Mandrus, D.; Taniguchi, T.; Watanabe, K.; Kitamura, K.; Yao, W.; et al. Electrically Tunable Excitonic Light-emitting Diodes based on Monolayer WSe_2 *pn* Junctions. *Nat. Nanotechnol.* **2014**, *9*, 268−272.
(7) Mak, K. F.; Lee, C.; Hone, J.; Shan, J.; Heinz, T. F. Atomically Thin MoS_2: A New Direct-Gap Semiconductor. *Phys. Rev. Lett.* **2010**, *105*, 136805.
(8) Splendiani, A.; Sun, L.; Zhang, Y.; Li, T.; Kim, J.; Chim, C.-Y.; Galli, G.; Wang, F. Emerging Photoluminescence in Monolayer MoS_2. *Nano Lett.* **2010**, *10*, 1271−1275.
(9) Li, Z.; Ezhilarasu, G.; Chatzakis, I.; Dhall, R.; Chen, C.-C.; Cronin, S. B. Indirect Band Gap Emission by Hot Electron Injection in Metal/MoS_2 and Metal/WSe_2 Heterojunctions. *Nano Lett.* **2015**, *15*, 3977−3982.
(10) Liu, Y.; Wu, H.; Cheng, H. C.; Yang, S.; Zhu, E.; He, Q.; Ding, M.; Li, D.; Guo, J.; Weiss, N.; et al. Towards Barrier Free Contact to Molybdenum Disulfide using Graphene Electrodes. *Nano Lett.* **2015**, *15*, 3030.
(11) Choi, M. S.; Lee, G. H.; Yu, Y. J.; Lee, D. Y.; Lee, S. H.; Kim, P.; Hone, J.; Yoo, W. J. Controlled Charge Trapping by Molybdenum Disulphide and Graphene in Ultrathin Heterostructured Memory Devices. *Nat. Commun.* **2013**, *4*, 7.
(12) Lee, G. H.; Yu, Y. J.; Cui, X.; Petrone, N.; Lee, C. H.; Choi, M. S.; Lee, D. Y.; Lee, C.; Yoo, W. J.; Watanabe, K.; Taniguchi, T.; Nuckolls, C.; Kim, P.; Hone, J. Flexible and Transparent MoS_2 Field-Effect Transistors on Hexagonal Boron Nitride-Graphene Heterostructures. *ACS Nano* **2013**, *7*, 7931−7936.
(13) Cui, X.; Lee, G.-H.; Kim, Y. D.; Arefe, G.; Huang, P. Y.; Lee, C.-H.; Chenet, D. A.; Zhang, X.; Wang, L.; Ye, F.; et al. Multi-terminal Transport Measurements of MoS_2 Using a van der Waals Heterostructure Device Platform. *Nat. Nanotechnol.* **2015**, *10*, 534.
(14) Perera, M. M.; Lin, M.-W.; Chuang, H.-J.; Chamlagain, B. P.; Wang, C.; Tan, X.; Cheng, M. M.-C.; Tománek, D.; Zhou, Z. Improved Carrier Mobility in Few-layer MoS_2 Field-effect Transistors with Ionic-liquid Gating. *ACS Nano* **2013**, *7*, 4449−4458.
(15) Li, Z.; Chang, S.-W.; Chen, C.-C.; Cronin, S. B. Enhanced Photocurrent and Photoluminescence Spectra in MoS2 under Ionic Liquid Gating. *Nano Res.* **2014**, *7*, 973−980.
(16) Yamamoto, M.; Dutta, S.; Aikawa, S.; Nakaharai, S.; Wakabayashi, K.; Fuhrer, M. S.; Ueno, K.; Tsukagoshi, K. Self-Limiting Layer-by-Layer Oxidation of Atomically Thin WSe_2. *Nano Lett.* **2015**, *15*, 2067−2073.
(17) Anthony, B.; Breaux, L.; Hsu, T.; Banerjee, S.; Tasch, A. *In situ* Cleaning of Silicon Substrate Surfaces by Remote Plasma-excited Hydrogen. *J. Vac. Sci. Technol., B: Microelectron. Process. Phenom.* **1989**, *7*, 621−626.
(18) Zhang, G.; Qi, P.; Wang, X.; Lu, Y.; Li, X.; Tu, R.; Bangsaruntip, S.; Mann, D.; Zhang, L.; Dai, H. Selective Etching of Metallic Carbon Nanotubes by Gas-phase Reaction. *Science (Washington, DC, U. S.)* **2006**, *314*, 974−977.

DOI: 10.1021/acsnano.6b02488
ACS Nano 2016, 10, 6836−6842

(19) Dhall, R.; Neupane, M. R.; Wickramaratne, D.; Mecklenburg, M.; Li, Z.; Moore, C.; Lake, R. K.; Cronin, S. Direct Bandgap Transition in Many-Layer MoS_2 by Plasma-Induced Layer Decoupling. *Adv. Mater. (Weinheim, Ger.)* **2015**, *27*, 1573.
(20) Tonndorf, P.; Schmidt, R.; Böttger, P.; Zhang, X.; Börner, J.; Liebig, A.; Albrecht, M.; Kloc, C.; Gordan, O.; Zahn, D. R.; et al. Photoluminescence Emission and Raman Response of Monolayer MoS_2, $MoSe_2$, and WSe_2. *Opt. Express* **2013**, *21*, 4908−4916.
(21) del Corro, E.; Terrones, H.; Elias, A.; Fantini, C.; Feng, S.; Nguyen, M. A.; Mallouk, T. E.; Terrones, M.; Pimenta, M. A. Excited Excitonic States in 1L, 2L, 3L, and Bulk WSe_2 Observed by Resonant Raman Spectroscopy. *ACS Nano* **2014**, *8*, 9629−9635.
(22) Zhao, W.; Ghorannevis, Z.; Chu, L.; Toh, M.; Kloc, C.; Tan, P.-H.; Eda, G. Evolution of Electronic Structure in Atomically Thin Sheets of WS_2 and WSe_2. *ACS Nano* **2013**, *7*, 791−797.
(23) Luo, X.; Zhao, Y.; Zhang, J.; Toh, M.; Kloc, C.; Xiong, Q.; Quek, S. Y. Effects of Lower Symmetry and Dimensionality on Raman Spectra in Two-dimensional WSe_2. *Phys. Rev. B: Condens. Matter Mater. Phys.* **2013**, *88*, 195313.
(24) Park, J.; Choudhary, N.; Smith, J.; Lee, G.; Kim, M.; Choi, W. Thickness Modulated MoS_2 Grown by Chemical Vapor Deposition for Transparent and Flexible Electronic Devices. *Appl. Phys. Lett.* **2015**, *106*, 012104.
(25) Nemes-Incze, P.; Osváth, Z.; Kamarás, K.; Biró, L. Anomalies in Thickness Measurements of Graphene and Few Layer Graphite Crystals by Tapping Mode Atomic Force Microscopy. *Carbon* **2008**, *46*, 1435−1442.
(26) Novoselov, K. S.; Geim, A. K.; Morozov, S.; Jiang, D.; Zhang, Y.; Dubonos, S. a.; Grigorieva, I.; Firsov, A. Electric Field Effect in Atomically Thin Carbon Films. *Science (Washington, DC, U. S.)* **2004**, *306*, 666−669.
(27) Lee, C.; Yan, H.; Brus, L. E.; Heinz, T. F.; Hone, J.; Ryu, S. Anomalous Lattice Vibrations of Single- and Few-Layer MoS_2. *ACS Nano* **2010**, *4*, 2695−2700.
(28) McDonnell, S.; Brennan, B.; Azcatl, A.; Lu, N.; Dong, H.; Buie, C.; Kim, J.; Hinkle, C. L.; Kim, M. J.; Wallace, R. M. HfO_2 on MoS_2 by Atomic Layer Deposition: Adsorption Mechanisms and Thickness Scalability. *ACS Nano* **2013**, *7*, 10354−10361.
(29) Pouzet, J.; Bernede, J. C.; Khellil, A.; Essaidi, H.; Benhida, S. Preparation and Characterization of Tungsten Diselenide Thin-films. *Thin Solid Films* **1992**, *208*, 252−259.
(30) Biloen, P.; Pott, G. X-ray Photoelectron Spectroscopy Study of Supported Tungsten Oxide. *J. Catal.* **1973**, *30*, 169−174.
(31) Jaegermann, W.; Schmeisser, D. Reactivity of Layer Type Transition Metal Chalcogenides towards Oxidation. *Surf. Sci.* **1986**, *165*, 143−160.
(32) Tenne, R.; Eherman, K.; Mahalu, D.; Peisach, M.; Kautek, W.; Wold, A.; Matson, R.; Waldeck, D. H. The WSe_2 Tungsten-oxide Interface - Structure and Photoluminescence. *Ber. Bunsen-Ges. Phys. Chem. Chem. Phys.* **1993**, *97*, 702−709.
(33) Yang, X.; Tang, S.; Ding, G.; Xie, X.; Jiang, M.; Huang, F. Layer-by-layer Thinning of Graphene by Plasma Irradiation and Post-annealing. *Nanotechnology* **2012**, *23*, 025704.
(34) Liu, Y.; Nan, H.; Wu, X.; Pan, W.; Wang, W.; Bai, J.; Zhao, W.; Sun, L.; Wang, X.; Ni, Z. Layer-by-layer Thinning of MoS2 by Plasma. *ACS Nano* **2013**, *7*, 4202−4209.
(35) Dimiev, A.; Kosynkin, D. V.; Sinitskii, A.; Slesarev, A.; Sun, Z.; Tour, J. M. Layer-by-layer Removal of Graphene for Device Patterning. *Science (Washington, DC, U. S.)* **2011**, *331*, 1168−1172.
(36) Chuang, S.; Battaglia, C.; Azcatl, A.; McDonnell, S.; Kang, J. S.; Yin, X.; Tosun, M.; Kapadia, R.; Fang, H.; Wallace, R. M.; et al. MoS_2 P-type Transistors and Diodes Enabled by High Work Function MoOx Contacts. *Nano Lett.* **2014**, *14*, 1337−1342.
(37) Kim, S.; Nah, J.; Jo, I.; Shahrjerdi, D.; Colombo, L.; Yao, Z.; Tutuc, E.; Banerjee, S. K. Realization of a High Mobility Dual-gated Graphene Field-effect Transistor with Al_2O_3 Dielectric. *Appl. Phys. Lett.* **2009**, *94*, 062107.

DOI: 10.1021/acsnano.6b02488
ACS Nano 2016, 10, 6836−6842